Validation of Multiphase CFD Predictions of the SLS Launch Environment against Artemis I Flight Data

T. Rivord[1] and B. Williams.[2]
NASA Marshall Space Flight Center, Huntsville, AL, USA

I. Introduction

A. SLS Launch Environment Overview

NASA's Space Launch System (SLS) is powered by four Aerojet-Rocketdyne RS-25 engines, previously referred to as Space Shuttle Main Engines (SSMEs), with two RSRMV solid rocket boosters (SRBs) derived from the Shuttle booster as seen in Fig. 1. Ignition and the start transient of the SRBs, each of which generate 3.6 million pounds of thrust, create a series of large magnitude pressure waves separate from launch acoustics that have the potential to damage the vehicle if unmitigated. This portion of the SLS launch environment consists of igniter shock (IS), ignition overpressure (IOP), and duct overpressure (DOP).

Fig. 1 SLS Block 1 10008 Vehicle Configuration.

Igniter shock is the first pressure wave to leave the SRB nozzle during the ignition transient and is caused by activation of the motor's igniter at the head end. The pressure wave originating from the igniter travels down the length of the motor and through the nozzle ahead of the SRB combustion gases. After leaving the nozzle, the IS wave impacts surrounding structures, which must withstand the resulting loading as this portion of the environment is not mitigated. A depiction of SRB igniter shock is provided in Fig. 2.

[1] CFD Analyst, NASA MSFC ER42, travis.a.rivord@nasa.gov
[2] CFD Team Lead, NASA MSFC ER42, brandon.williams@nasa.gov

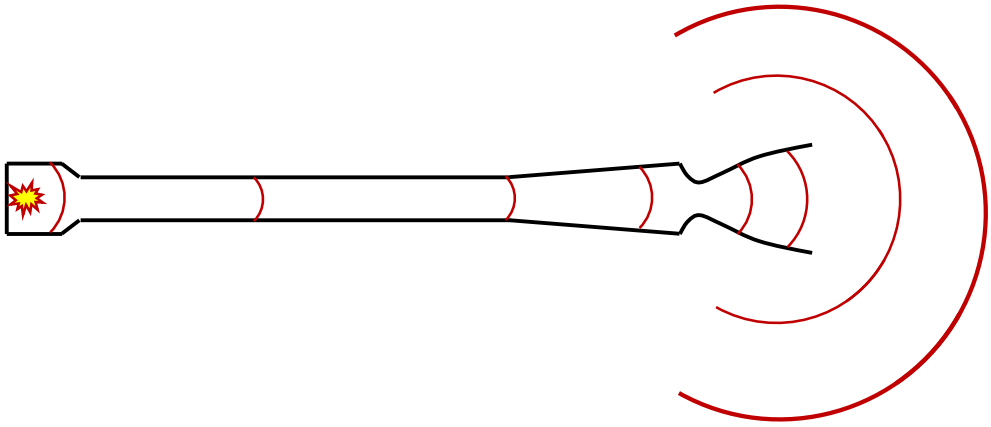

Fig. 2 Depiction of SRB igniter shock propagation.

Following IS, the SRB combustion gases (i.e., plume) flow through the nozzle and into the mobile launcher hole (MLH) duct. The rapid acceleration of the plume compresses the ambient air in the confined duct, forming a pressure source as depicted in Fig. 3. A common analogy for this is a piston (the SRB plume) displacing air in a cylinder (the MLH duct). When no mitigation efforts are taken, this source releases near the bottom of the MLH and the portion traveling upwards towards the vehicle is labeled ignition overpressure (IOP) while the portion traveling downwards becomes a part of duct overpressure (DOP). It is important to note that the confined SLS geometry, with the plumes contained by the MLH duct, has a first order effect on the formation of the IOP pressure source and resulting overpressure magnitude; without the confined duct, the overpressure source would be significantly smaller. The formation and propagation of DOP is not the focus of this paper.

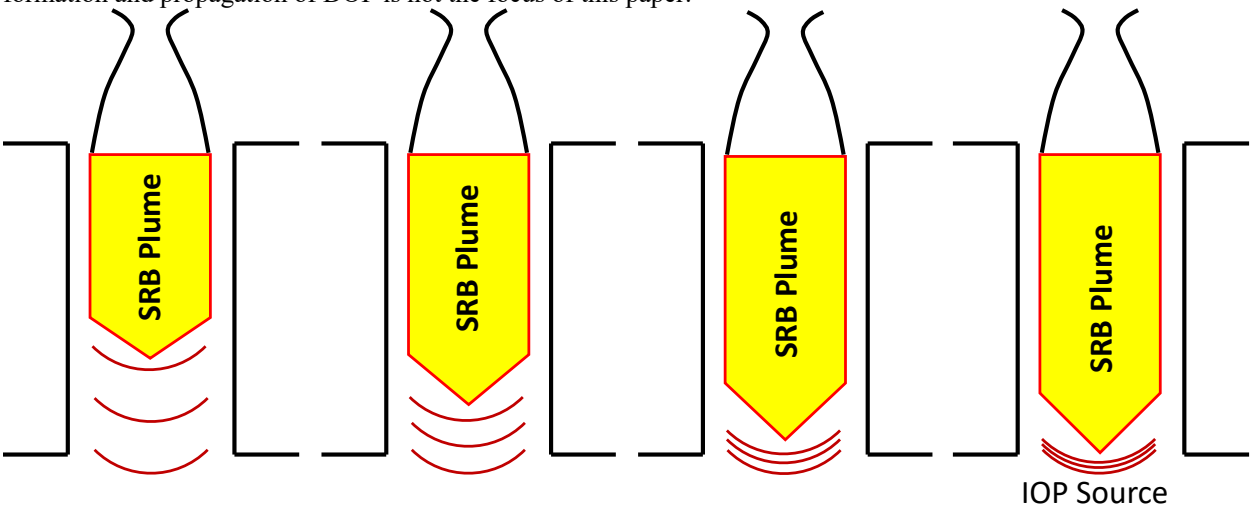

Fig. 3 Depiction of SRB ignition overpressure source formation.

The igniter shock environment is not targeted with any mitigation; the surrounding structures exposed to the environment are designed to withstand the resulting loads. The IOP environment, which has the potential to cause significant damage to the vehicle and crew, is mitigated by injecting large quantities of water beneath the SRB nozzle based on prior experience with the Shuttle Program.

Prior to the first Space Shuttle mission, STS-1, no mitigation efforts were implemented to reduce the magnitude of the IOP waves. During the STS-1 launch, the SRB generated IOP waves caused structural damage to the Shuttle vehicle and was reported to be felt by the astronauts and motivated an effort to mitigate IOP prior to STS-2. It was known that water reduced the amplitude of acoustics, so a subscale test series was executed to determine whether water could also reduce the magnitude of IOP. The testing indicated that the addition of water would reduce IOP magnitude, though the exact mechanism for this reduction was unknown. The IOP water mitigation was implemented on the launchpad and found to be successful during the next launch, STS-2 [1].

Building on Shuttle experience, the SLS program includes an ignition overpressure/sound suppression (IOP/SS) water system on the mobile launcher to protect the SLS vehicle from IOP and other acoustic loads as pictured in Fig. 4. The water is injected very close to the nozzle exit planes as the Shuttle era subscale testing indicated this maximized the water's effectiveness. The SRB plumes, the proximity of the IOP/SS water, and the liquid engine plumes create a complex multiphase environment during the SRB ignition transient resulting in many unintended consequences including water spray, potential debris transport, and strong plume-water interaction.

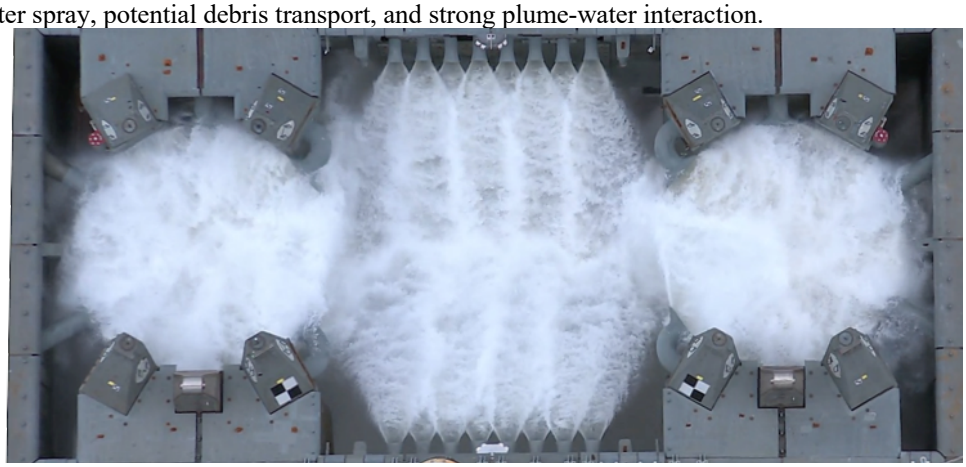

Fig. 4 Top-down view of the SLS IOP/SS water system.

A subscale test series, scale model acoustic test (SMAT), was conducted to verify the effectiveness of the SLS IOP/SS water configuration for IOP mitigation. This test, combined with heritage Shuttle Program data, gave confidence in the water system's effectiveness and the developed launch environment. There was, however, some uncertainty regarding the launch environment due to configuration differences between Shuttle and SLS, particularly the SRB plume-water interaction for the full scale SLS configuration. Because no full integrated system SLS testing was conducted prior to launch, computational fluid dynamics (CFD) was relied upon to inform the SLS program on the multiphase launch environment.

In the last decade, the multiphase computational fluid dynamics (CFD) tools Loci/CHEM real fluids (RF) and Loci/STREAM-Volume of Fluid (VoF) were developed to enable simulations of the full launch environment. These simulations (five in total) were extensively used to support the SLS program including but not limited to RS-25 lead hydrogen burn-off igniters (HBOIs) operation, water system design, debris transport, and environment development. However, validation of these CFD tools on the launch environment were limited to individual SLS system tests [2]. In the year following Artemis I, CFD predictions have been extensively examined and compared to flight data and video. The purpose of this paper is to present validation of the multiphase CFD solvers Loci/CHEM-RF and Loci/STREAM-VoF against the launch environment by comparing CFD predictions against Artemis I flight video and pressure data on the SLS vehicle.

B. CFD Multiphase Models Applied to Launch Environment

The MSFC team has fielded two different fidelity two-phase models in past analyses. The first is the 'lower fidelity' diffuse interface Real Fluid (RF) model implemented into the Loci/CHEM density-based solver. The second is the 'higher fidelity' sharp interface geometric Volume of Fluid (VoF) model implemented into the Loci/STREAM pressure-based solver.

The Loci/CHEM-RF model does not explicitly track or model the details of the gas-liquid interface. Because of this, surface tension is not included, droplets and ligaments of liquid are not resolved, and the liquid in interfacial regions is allowed to mix and diffuse in a non-physical manner. In the RF model, the liquid essentially acts as a 'heavy gas' with appropriate thermodynamic and phase change properties; were a droplet initialized in a quiescent domain free of body forces, it would eventually diffuse to fill the domain. While the RF model was not intended for this type of launchpad application, it has shown reasonable results in certain problems where interface details are not important and timescales of numerical diffusion are much longer than fluid convective timescales.

The Loci/STREAM-VoF model explicitly tracks the gas-liquid interface through geometric reconstruction. Because of this, surface tension can be applied to the interface and liquid structures properly breakdown to smaller droplets in response to external forces. The VoF model is close to a physical representation of liquid; were a droplet initialized in a quiescent domain free of body forces, the droplet would hold together as expected of a liquid. Throughout the development of the Loci/STREAM VoF code it has been extensively validated against canonical

problems. While the VoF model is high-fidelity, it has stringent mesh resolution requirements for accuracy and is computationally expensive; both accuracy and expense scales with the number of interfacial cells.

Comparative simulations of the SLS launchpad water are presented in Fig. 5 with the RF solution on the left and the VoF solution on the right. The slice is a log scale of density through the SRB centerline, which highlights the differences between the models. VoF captures the appropriate density of liquid water (1,000 kg/s) and discrete liquid structures while RF captures the general location of the water, but neither the density of liquid water nor discrete drops of water. A major limitation of the VoF model is that the scale of liquid structures is directly correlated to the mesh size; the existing water structures should breakup into smaller droplets via Weber number breakup, but the existing mesh resolution does not allow this. The capability of these models, each with their own limitations, to predict the multiphase SLS launch environment is the focus of this paper.

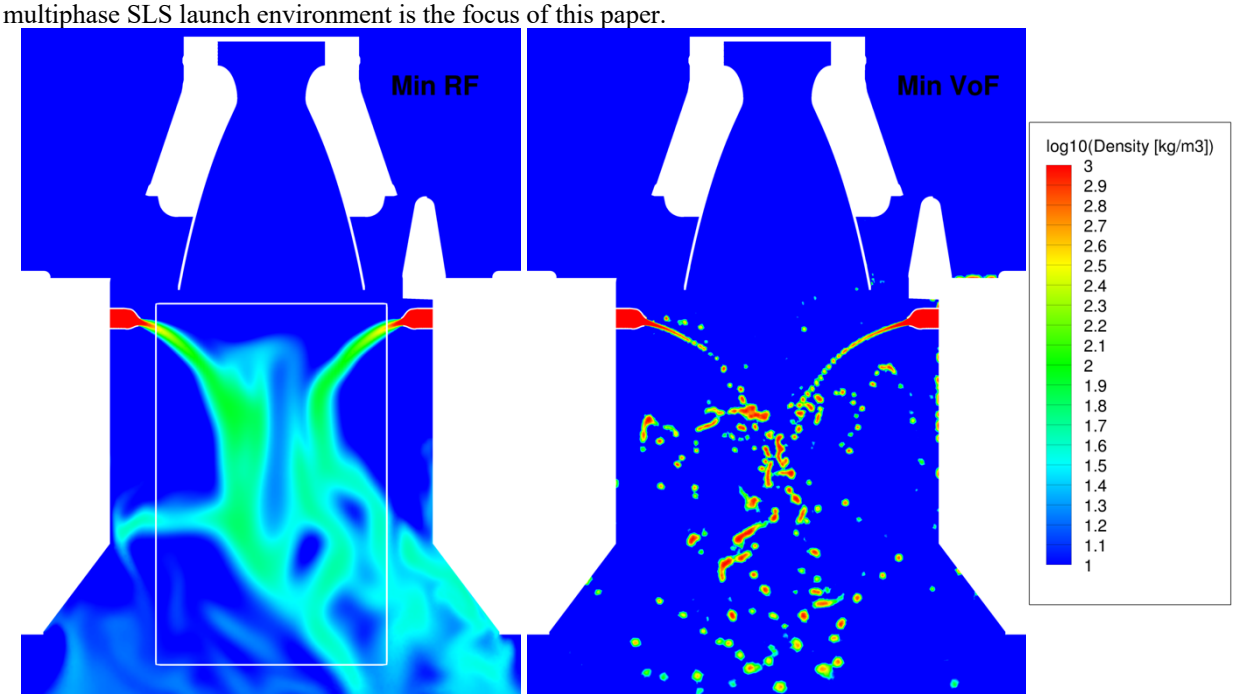

Fig. 5 Comparison of RF (left) and VoF (right) models for two density contour ranges.

II. Computational Model

A. Simulation Overview

The SLS ignition sequence occurs in three distinct steps. First, the IOP/SS water is activated and reaches a steady state prior to RS-25 ignition. Next, approximately six seconds prior to T0, the RS-25 engines ignite reaching 100% rated power level (RPL) after four seconds. Lastly, the SRB ignition is initiated at T0, though it takes approximately 0.1 seconds for the igniter shock to travel the length of the booster.

All CFD simulations were conducted in three similar phases to mimic the physical launch sequence. First, the IOP/SS water was developed to a quasi-steady state. Next, the RS-25 engines were activated and ramped to 100% RPL and lastly, the SRB was activated. There are slight differences between how the CFD simulations were conducted, but the flowfield prior to SRB ignition is expected to be equivalent to conditions that will occur during launch. While all three phases of the launch environment were simulated, only the final portion, the SRB ignition transient, is examined presently.

The five existing CFD predictions of the SLS multiphase launch environment were executed with various SRB propellant mean bulk temperatures (PMBT), which affect Booster ignition transient timing, and IOP/SS water flowrates, which affect the intensity of the plume-water interaction. It was decided to focus on the simulations most representative of flight conditions in this paper. The three simulations using the high PMBT Booster ignition transient from the Demonstration Motor 1 (DM-1) static test were selected as they were closest to the flight temperature. Two simulations (one RF and one VoF) used IOP/SS water flowrates based on the Integrated System Verification and Validation 14 (ISVV-14) test series of the IOP/SS system at Kennedy Space Center (KSC), which is considered a lower bound on the flight water flowrates. These simulations will be referred to by “Min RF” and “Min VoF” from

here on. The third simulation, executed with RF, used an earlier prediction of peak maximum IOP/SS water flowrates referred to as "Max RF." The actual Artemis I water flowrates are bounded by the ISVV-14 and max water flowrate simulations. It should be noted that only the Min RF simulation includes the water injected on top of the main flame deflector (MFD) in the north flame trench. The implications of this will be discussed later

B. Computational Domain and Mesh

The computational geometry for all three simulations was generated using a combination of the SLS geometry from [3], the verified CAD model of the ML [4], and the IOP/SS geometry provided by Exploration Ground Systems (EGS) [5]. On the ML, only those features expected to affect the IOP/SS water flow and initial plume environment were retained, and many of those were simplified. Only the aft portion of the SLS vehicle was modeled as only this portion will interact with the IOP/SS water. These geometry modifications were made to reduce the mesh size and complexity. To further reduce the computational expense of the simulation, a symmetry boundary condition was placed at the vehicle centerline. Though the presence of the symmetry plane is not thought to significantly affect the results from the present simulations, this needs to be investigated further. The final computational domain and geometry for the SLS multiphase launch environment simulations is provided in Fig. 6.

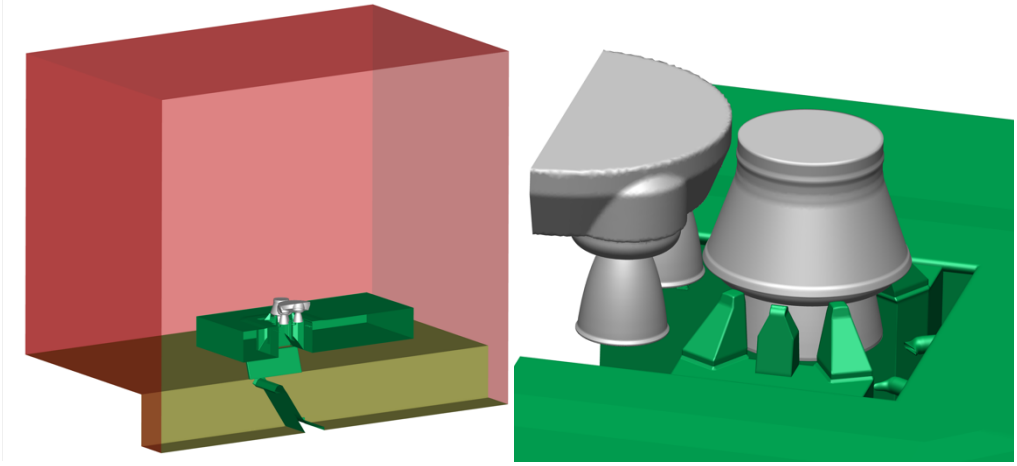

Fig. 6 Simulation computational domain and geometry.

Each of the three CFD simulations examined presently used a different computational mesh. The distribution of cells for each of the meshes is demonstrated by Fig. 7 which shows the characteristic length scales of the meshes, calculated as the cube-root of the cell volume, on vertical cutting planes through the SRB centerline. As the focus of these simulations was on the interaction of the SLS rocket plumes and IOP/SS water, the bulk of the mesh density was targeted to capture the water features and interactions in those regions.

The Min VoF mesh targeted the region under the SRB nozzle with a mesh edge length of 1.5", increasing to 2" at the bottom of the MLH while the region under the RS-25 nozzles was targeted with a mesh edge length of 1", increasing to 2" at the bottom of the MLH. To reduce VoF Courant number restrictions on the timestep, a severe penalty on computational efficiency, a prism layer was only included on the RS-25 and SRB nozzle surfaces. The effect of under-resolving the boundary layer on other viscous wall surfaces has yet to be determined, but is expected to be relatively small for the water-water and plume-water interactions which are the primary metrics of interest.

Both RF simulations used equivalent meshes near the vehicle and in the MLH. The primary difference between the two RF meshes is that the Min RF mesh maintains mesh resolution in the trench under the mobile launcher while the Max RF mesh rapidly coarsens the mesh. This is anticipated to have little effect on the metrics examined in this paper. Both RF meshes target the mesh edge length within the MLH to 2" and grow prism layers on all solid walls to enable resolution of a viscous boundary layer.

For all meshes, except where mentioned, regions outside of the MLH grow rapidly to reduce mesh cell count and dissipate pressure waves prior to hitting farfield boundaries. The final mesh cell counts for the Min VoF, Min RF, and Max RF meshes are approximately 91 million, 86 million, and 56 million, respectively.

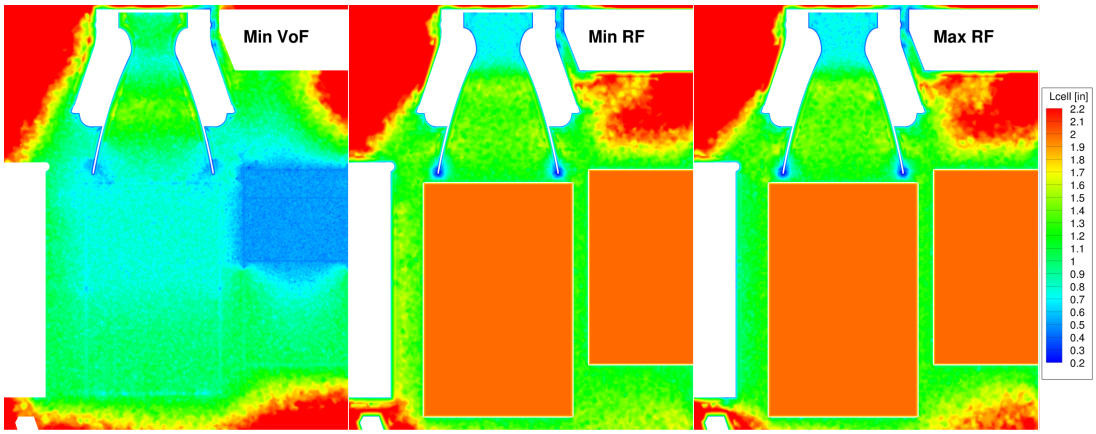

Fig. 7 Characteristic cell lengths on cutting planes through the SRB centerline for the Min VoF (left), Min RF (middle), and Max RF (right) simulations.

C. Computational Settings

The Loci/STREAM-VoF simulation was executed with second order spatial and first order temporal accuracy. The inviscid flux scheme applied is second order upwinding with the Venkatakrishnan limiter. The simulation was executed with the delayed detached eddy simulation (DDES) turbulence model. All walls were set to viscous walls using wall functions, though only the RS-25 and SRB nozzle surfaces have a prism layer to resolve the boundary layer.

Both Loci/CHEM-RF simulations used identical numerical settings. They were executed with second order spatial and second order temporal accuracy. The inviscid flux scheme applied is the HLLE (Harten-Lax-van Leer-Einfeldt) flux scheme formulated with Chorin-Turkel (CT) local preconditioning scheme. Generally, the HLLE flux scheme is regarded as dissipative, at least compared to the stiffer Roe flux scheme. The simulation was executed with a hybrid Reynold-averaged Navier-Stokes (RANS)-large eddy simulation (LES) turbulence model. All walls were set to viscous walls. The prism layer on each surface was resolved sufficiently to capture the boundary layer without the use of wall functions.

III. Analysis

The validation of the CFD simulations against Artemis I flight data consists of both quantitative and qualitative validation. Qualitative validation is conducted by comparing CFD flow field visualizations to flight events observed on high-speed videos. These comparisons are limited for Artemis I because due to quality issues with imagery and the launch occurring at night. Quantitative validation is conducted by comparing CFD predictions of pressure to recorded flight pressure data.

A. CFD Qualitative Validation: Observed Launch Events

A sequence of images from an Artemis I high-speed digital camera on the mobile launcher tower looking downwards captures the plume-water interaction that occurs during SRB ignition, and compares the flow dynamics with the CFD simulations in Fig. 8. In this series, time increases from top to bottom. The first image from the left is cropped from launch camera 30-P2, the second image is of the Min VoF CFD flowfield, the third is of the Min RF CFD flowfield, and the right image is of the Max RF CFD flowfield. The CFD images represent the water as a density iso-line on a velocity magnitude slice between the west Booster and Core Stage Engine (CSE) 2 centerlines. Note that the white boxes on the RF CFD images are an artifact of the rendering software, not an object in the flowfield. Because of the variability in the SRB ignition transient, the timing of the launch imagery and the CFD simulations are aligned to the appearance of the IS wave at the nozzle exit, which will be referred to as IS+0 ms in the remainder of this section. All subsequent times for this comparison are provided as deltas from this event.

The igniter shock ring can be seen leaving the Artemis I Booster nozzle at IS+4 ms. This ring, also observed during SRB static fires, is caused by diffraction of the igniter shock flow around the SRB nozzle lip. The ring vortex lowers the humid air's local temperature below that of the saturation point, causing the water vapor to condense. The IS ring is present in the CFD simulations, shown by the recirculating ring vortex attached to the nozzle lip. Following the IS ring, the SRB plume begins to emerge from the nozzle and stagnate on the IOP/SS water. The plume does not have

enough momentum to displace the dense water sheets initially, resulting in the flow turning outwards in all directions. This outward turn occurs by IS+12 ms.

At IS+20 ms, the outward flow impacts CSE-2 in the launch imagery and within a few milliseconds of this for all CFD simulations. As the plume continues to develop, the flow transitions from outwards (towards the RS-25 engine) to upwards (towards the vehicle base) as seen at IS+25 ms. The CFD simulations indicate that the water sheets begin to deform as the SRB flow continues to stagnate on their surface. The deformed water sheets create a bowl shape, redirecting the outward flow up toward the vehicle base.

Overall, the plume-water interaction transport mechanism observed in flight is qualitatively captured by all three CFD simulations. This is considered successful qualitative validation of the Loci/CHEM-RF and Loci/STREAM-VoF CFD solvers for the early portions of the SLS launch environment.

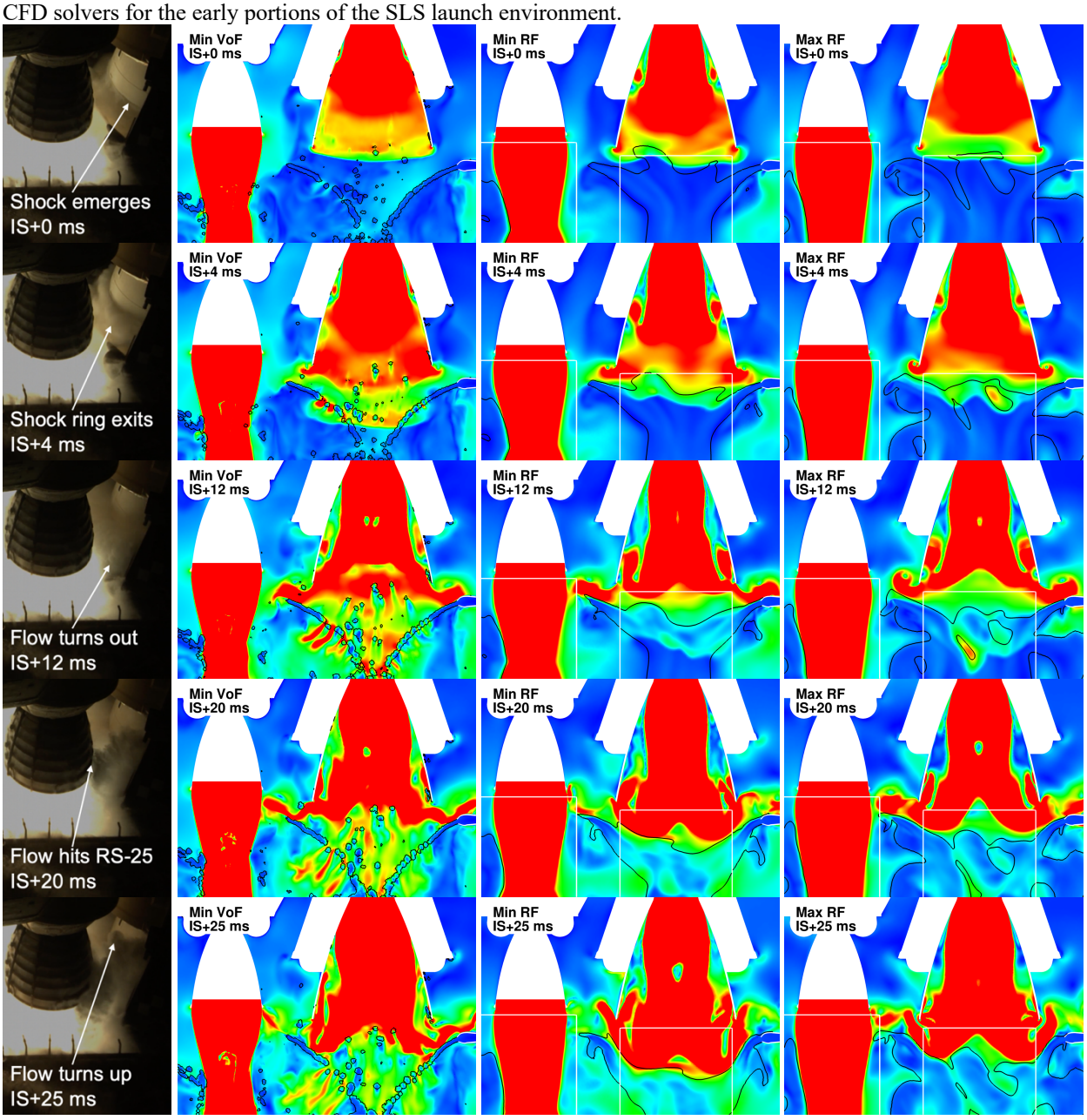

Fig. 8 Plume-water interaction qualitative comparison for Artemis I and the three CFD simulations.

B. CFD Quantitative Validation: Core Stage Base Pressure

As mentioned in the Introduction section, there are three large-magnitude pressure events separate from launch acoustics that are caused by SRB ignition and subsequent transient: igniter shock (IS), ignition overpressure (IOP), and duct overpressure (DOP). Igniter shock first leaves the nozzle ahead of the combustion gases as a result of the booster igniter activating. Ignition overpressure occurs later in the SRB transient as the developing plume of supersonic combustion gases compresses the ambient air confined in the MLH forming a large pressure source that releases upwards (IOP) and downwards (DOP). It should be noted that the pressure source resulting in the IOP and DOP waves is strongly affected by the confined MLH geometry; without that confinement, the pressure source, and resulting wave magnitude, would be significantly smaller. The downward traveling portion of the pressure source, DOP, is not discussed in this paper.

Artemis I pressure data measured on the Core Stage (CS) base heat shield is provided in Fig. 9 without filtering through the first portion of the SRB ignition sequence. First flow through the SRB nozzle occurs approximately at the left-hand side of the x-axis. The pressure transient has been split into ranges A through D for ease of discussion. Range A consists of acoustics generated by the RS-25 plumes that are active and at full power prior to SRB ignition. The RS-25 acoustics are relatively low magnitude and high frequency compared to the SRB generated pressure events. Range B contains the first pressure event caused by the SRB transient, igniter shock. There is one low frequency, high magnitude, pressure event at the probe location followed by a series of lower magnitude events. Ranges C and/or D are expected to contain IOP, but the Artemis I IOP signature did not align with expectations based on the Shuttle Program and subscale testing. Comparisons to the CFD pressure data and solutions will be used to shed insight on ranges C and D in the following paragraphs.

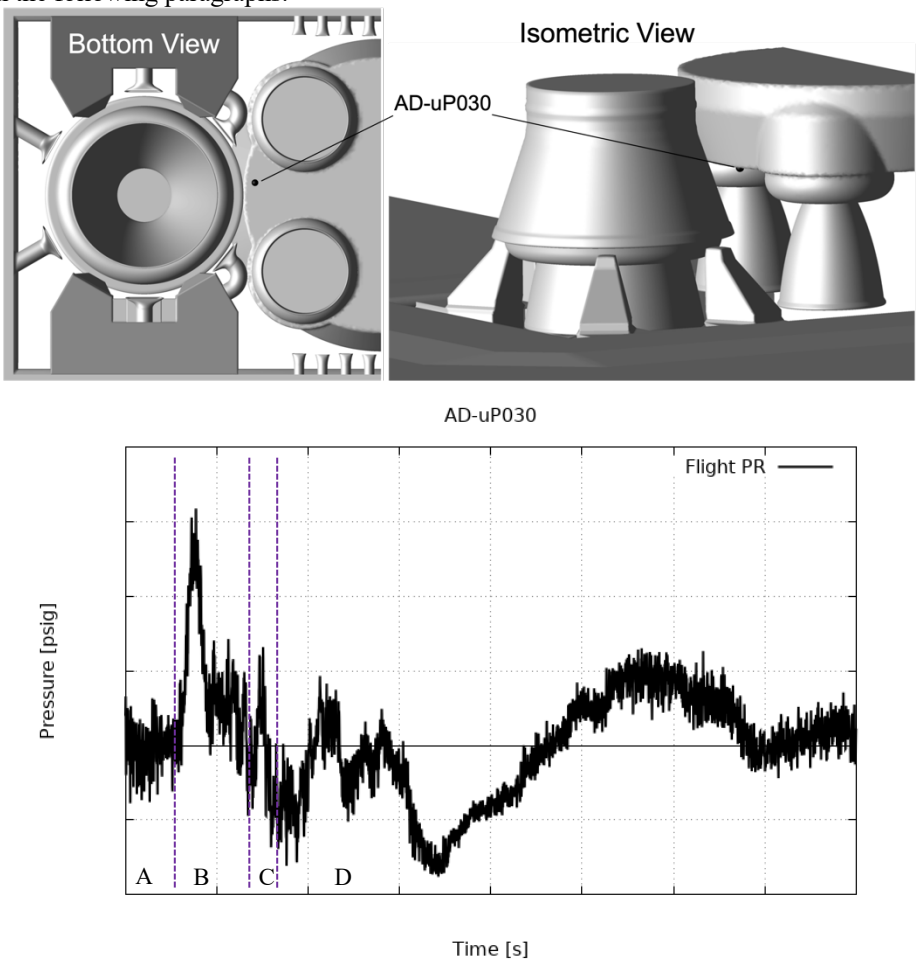

Fig. 9 Artemis I base heat shield probe (top) with pressure data (bottom).

The CFD simulation pressure traces at the equivalent flight probe location are added to the Artemis I data in Fig. 10 with the same four ranges labeled. Due to differences in booster timing and CFD simulations, it was decided to align all CFD simulation IS peaks with the Artemis I IS peak. It is reasonable to align the data this way because previous

IS validation efforts indicate that the CFD is capable of predicting the timing of the IS wave. It should be noted that the CFD pressure data is limited to a sample rate of ~2,000 Hz. At first glance, ranges A through C match the flight data well, with some discrepancies in range D. A closer investigation of the similarities and differences will follow.

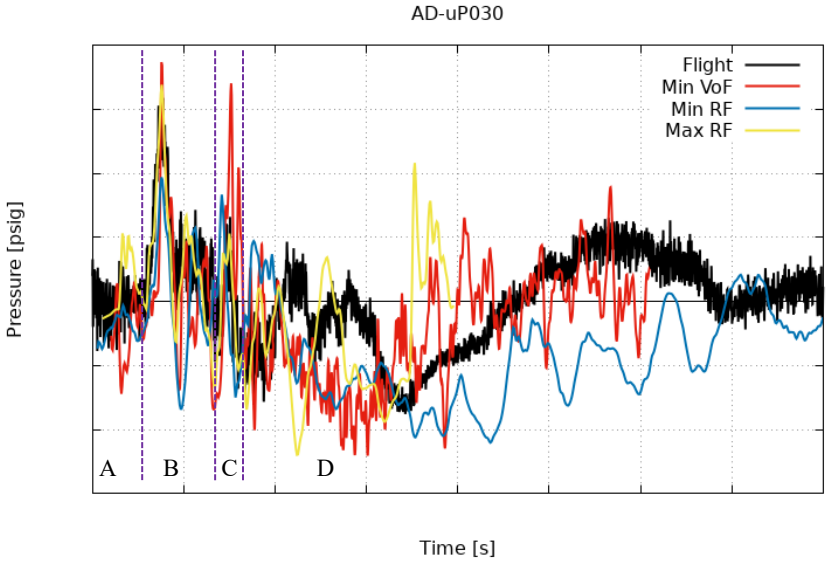

Fig. 10 Artemis I and shifted CFD base heat shield pressure data.

The time history for ranges A through C is provided in Fig. 11. During range A, none of the CFD signals contain the high frequency acoustics generated by the RS-25 engines. This could be a result of excess numerical and/or mesh induced dissipation in the CFD simulations as well as the ~2,000 Hz sampling rate of the CFD data. The 0.5 psig pressure signal in the Max RF pressure trace is a numerical artifact from the simulation process corrected for later simulations and not expected to corrupt the pressure data later in time.

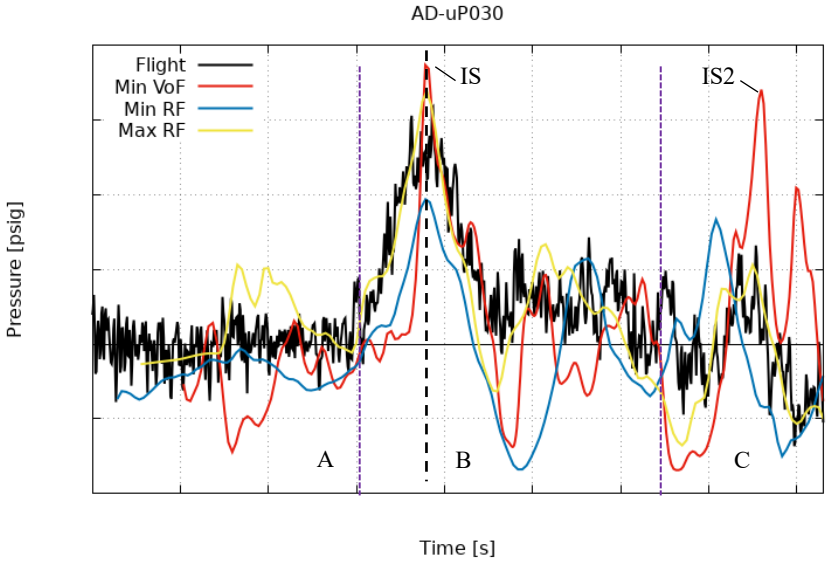

Fig. 11 Artemis I and shifted CFD base heat shield pressure data: Ranges A through C.

Range B contains the igniter shock event. All CFD simulations match the timing of IS due to the forced time-alignment based on this event. The Min VoF and Max RF simulations slightly overpredict the magnitude of IS while the Min RF simulation slightly underpredicts the magnitude. Following the largest magnitude wave in this range, there are a series of smaller pressure events. The flight data maintains an elevated pressure while the CFD captures both the positive and negative phases of these subsequent pressure waves. Overall, the IS portion of the SRB transient is well predicted by the both the Loci/CHEM-RF and Loci/STREAM-VoF CFD models.

A major benefit of CFD is that the flow fields can be investigated in detail to provide more insight into the physics occurring. This is done for the propagation of the IS wave from the SRB nozzle to the heat shield probe location in Fig. 12. Gauge pressure magnitude slices through the SRB centerline are provided with density iso-lines representing water for the three CFD solutions. The two RS-25s are located into/out of the page from this view. Simulation time increases from top to bottom in the figure, though the times are not necessarily aligned between the simulations.

The solutions show that the IS wave exits the SRB nozzle and encounters the IOP/SS water sheets. The IS wave continues to travel through the water, though a portion is reflected upwards towards the vehicle. The upward-reflected portion of IS impacts the heat shield in the last image of this sequence, which coincides with the peak magnitude in the pressure traces (dashed black line in Fig. 11). Though not shown here, the lower magnitude pressure signals following the large IS wave are a series of smaller IS waves originating from within the SRB nozzle.

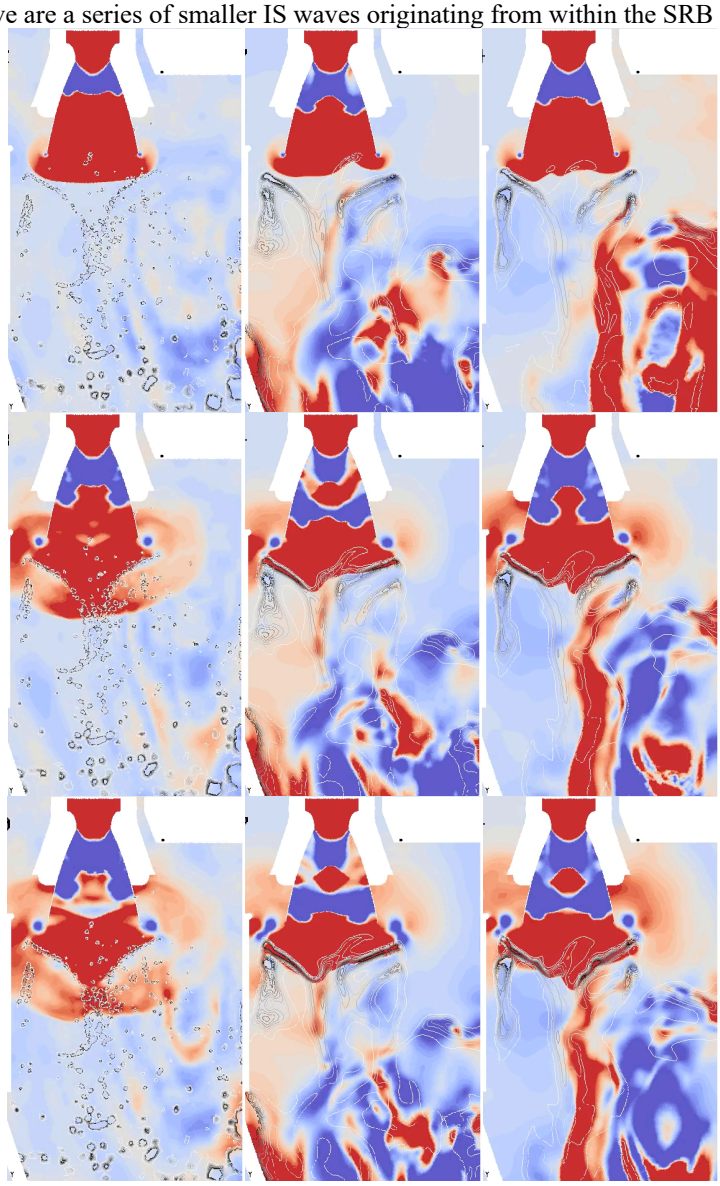

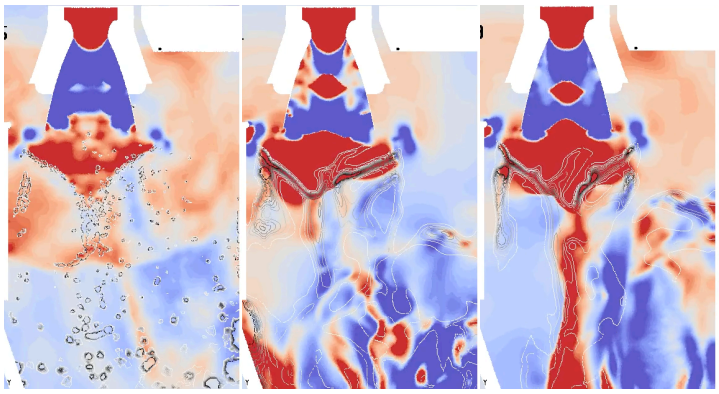

Fig. 12 Igniter shock propagation for Min VoF (left), Min RF (middle), and Max RF CFD solutions.

Range C contains an additional pressure event that was not accounted for in the defined SLS launch environment prior to the Artemis I flight. Examining the CFD solutions (Fig. 13) indicates that this pressure event emerges within the SRB nozzle, reflects off the water, then travels upwards to the base heat shield. Initially, it was thought that this wave might be due to the influence of water. Further examination, however, revealed that this overpressure wave exists in SRB static fire data *without* water. This means that the identified overpressure wave is a part of the SRB start-up transient and is a secondary igniter shock.

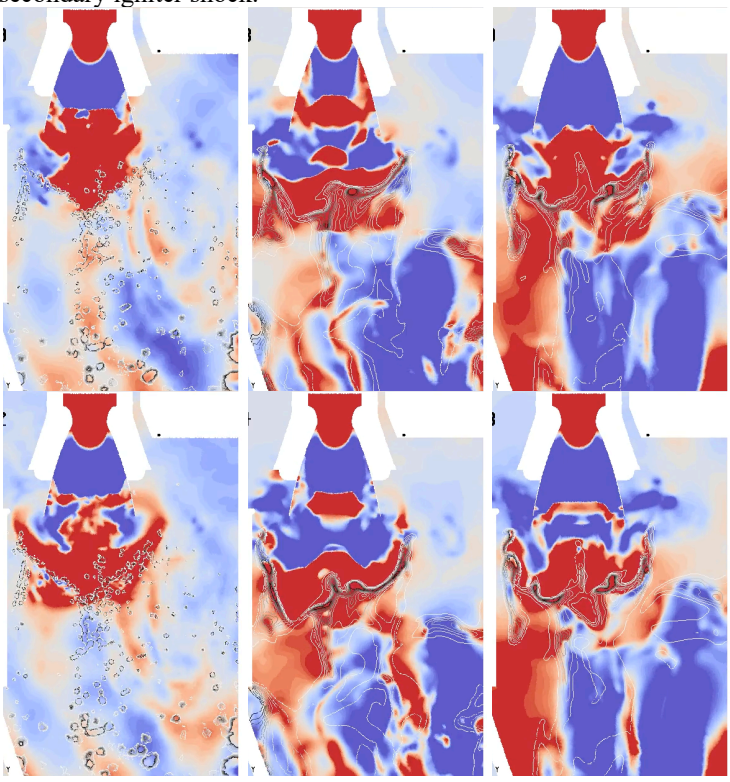

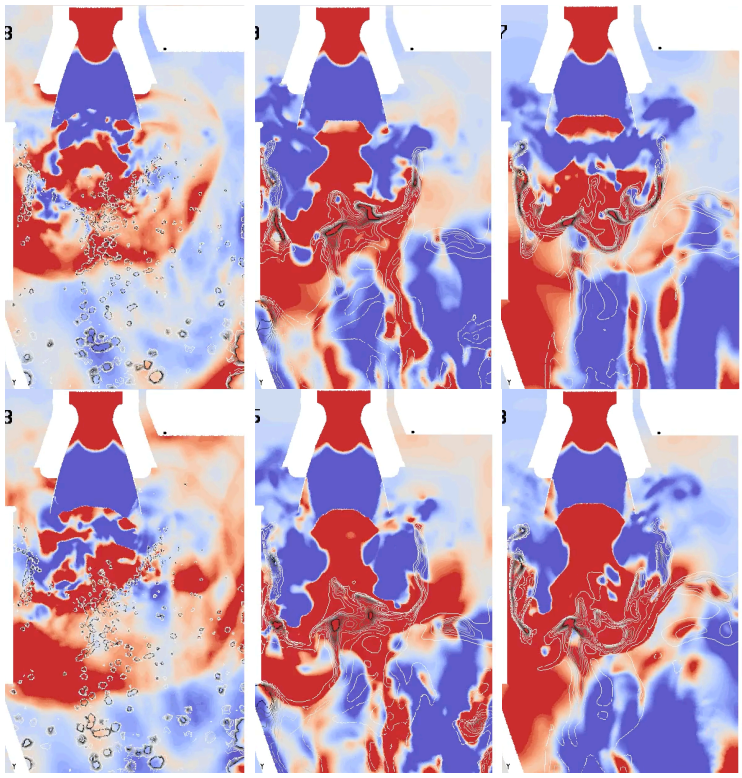

Fig. 13 Secondary igniter shock propagation for Min VoF (left), Min RF (middle), and Max RF CFD solutions.

The time history for range D is provided in Fig. 14. Since the wave identified in range C was determined to be a secondary igniter shock, IOP has to lie within range D. In the flight data, there is a vacuum pulled at the probe location with three positive magnitude pressure waves. The CFD data presents a similar trend; a vacuum interspersed with positive magnitude pressure events. Unlike the earlier pressure events, examining the CFD does not shed much insight on which wave (or waves) IOP could be. During this time range in the SLS launch sequence, the flow in the MLH consists of multiple supersonic jets that are interacting with water and impinging on the MLH side walls as well as multiple pressure waves from different sources reflecting and interacting with each other. This makes tracking the source of any pressure wave and its propagation path challenging. Four snapshots of the CFD flowfields are provided in Fig. 15, with solution times indicated by the vertical dashed lines in Fig. 14.

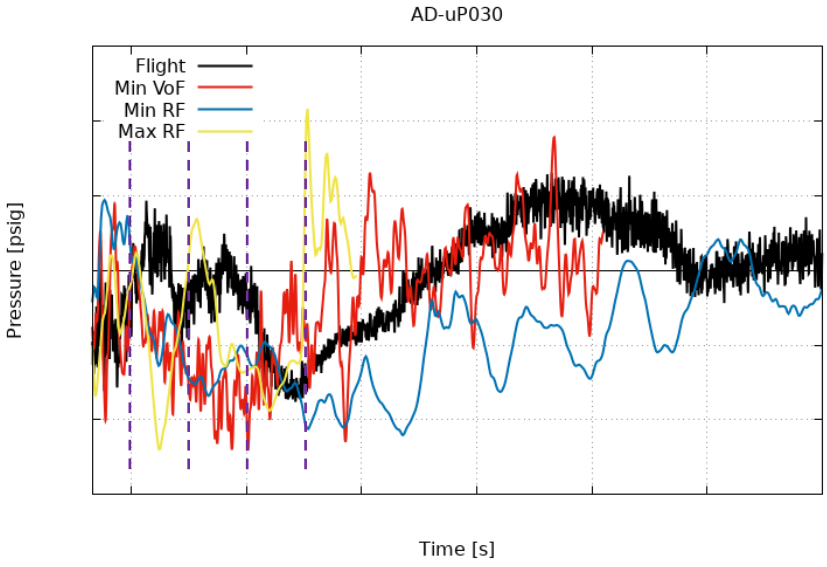

Fig. 14 Artemis I and shifted CFD base heat shield pressure data: Range D.

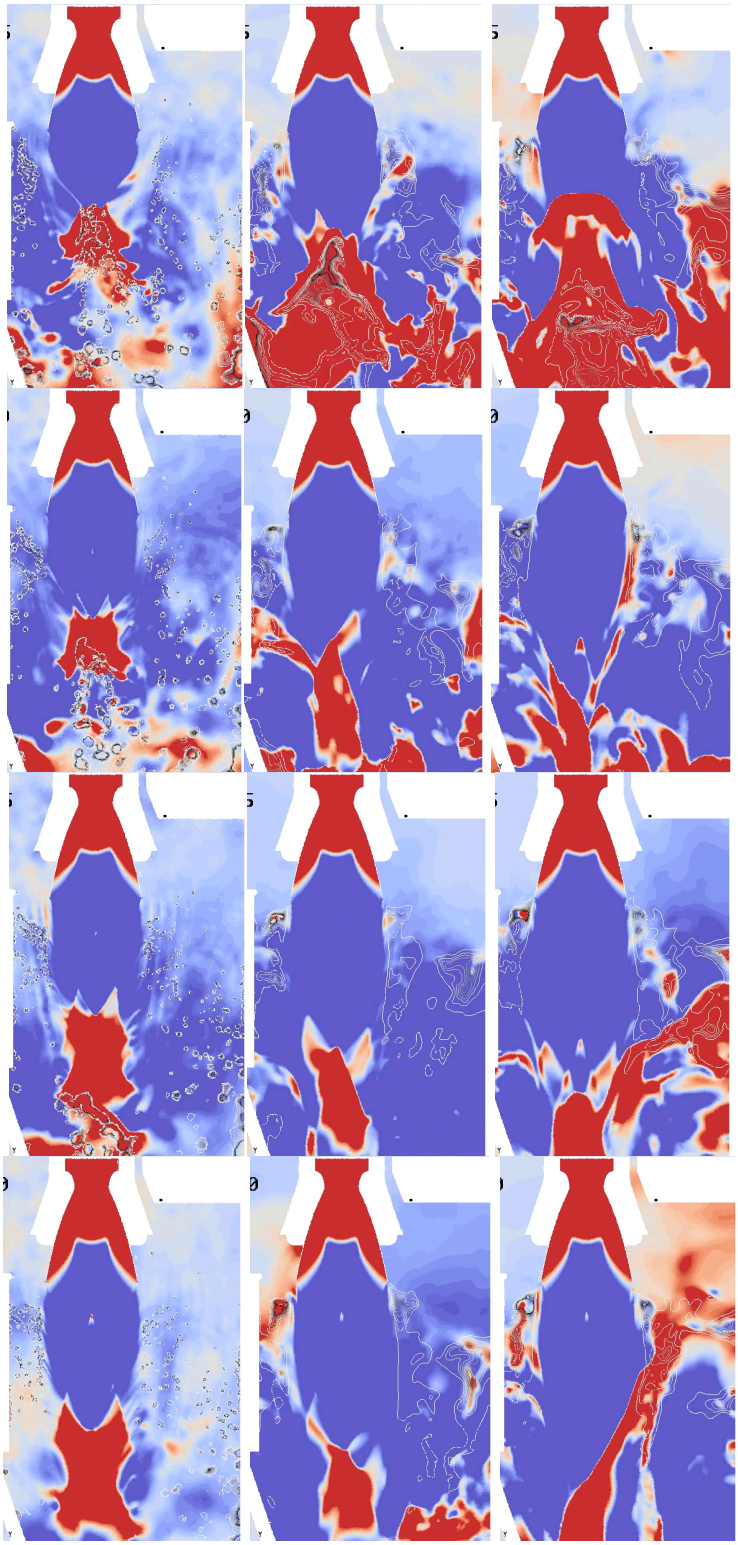

Fig. 15 Range D CFD solutions (possibly covering IOP) for Min VoF (left), Min RF (middle), and Max RF simulations.

As it is challenging to determine the IOP source and subsequent wave in the multiphase CFD simulations, it is useful to compare a CFD prediction of IOP *without* water to one with water. Base heat shield pressures during range D are compared for the Min RF simulation and an equivalent (numerical settings and computational mesh) simulation without water (i.e., dry) in Fig. 16. Though not obvious in the upon initial examination, there are actually two IOP waves present in the dry simulation. The first wave, labeled IOP1 is not immediately identifiable in the pressure data, but is apparent looking at the dry CFD solution (details to follow). The second dry wave, labeled IOP2, is approximately 6X the magnitude of the largest pressure wave in the Min RF simulation and approximately 2X larger than the dry IOP1. The reduction in pressure magnitudes from the dry to wet Min RF simulation qualitatively demonstrates the effectiveness of the modeled IOP/SS water system.

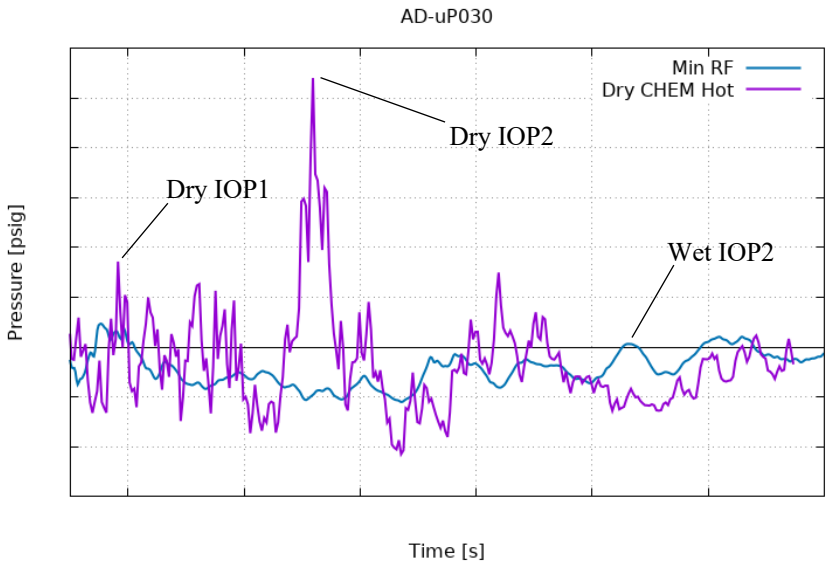

Fig. 16 Min RF CFD simulation base heat shield pressure data compared to equivalent simulation without water.

Gauge pressure, Mach number, and total temperature slices through the SRB centerline are provided in equal increments through the SRB transient for the dry simulation in Fig. 17 and wet Min RF simulation in Fig. 18. The time range selected includes the igniter shock flow through the formation of the IOP1 source identified in Fig. 16. The times shown for each solution are the same for both simulations, though additional times are provided for the wet Min RF simulation in Fig. 19. For all wet Min RF images, density iso-lines are provided to represent the water. It should be noted for both simulations that high total temperature corresponds to the location of the hot combustion gases of the SRB plume.

Focusing first on the dry simulation in Fig. 17, the first time shows that the cold igniter shock flow travels into the MLH ahead of the hot combustion gases. Here, the hot combustion gas from the igniter and the burning propellant at the head end of the SRB is pushing the ambient temperature air in the bore out through the nozzle, creating a relatively cold supersonic plume. This IS flow displays as a 'bloom' on the velocity slice circled in Fig. 17 where the head end of the plume is accelerating the air in the MLH. In the second time frame, the hot combustion gases still lag behind the IS flow bloom. The third time provided shows that the combustion gases have caught up to the IS flow and the plume's energy has intensified (higher total temperature). A pressure source forms near the bottom of the MLH and releases upwards (IOP) and downwards by the last time frame shown. This upwards travelling wave causes the IOP1 pressure signal labeled in Fig. 16.

Focusing now on the wet Min RF simulation in Fig. 18, the first time shows that the cold igniter shock flow travels into the MLH ahead of the hot combustion gases. This is similar to the dry simulation, though the water does impede the front of the IS flow. Additionally, the stagnation and outward turning of the IS flow does not form the same bloom of flow seen in the dry simulations because the plume cannot accelerate the denser water as quickly. Due to the hinderance of the water, the hot combustion gases have caught up to the IS flow by the second time, a frame earlier than in the dry simulation. The third frame shows that the plume's energy has intensified (higher total temperature), similarly to the dry simulation. By the last frame provided in Fig. 18, no pressure source has released and the plumes have yet to push through the end of the MLH due to the delay caused by the water. In the first frame of Fig. 19, a continuation in time, the pressure source finally releases. Notably, the source only releases in the downwards direction

and never appears to impact the base heat shield. It is possible that the blockage of the MLH by the supersonic plume and remaining water causes this wave to only release downwards, though more investigation is needed.

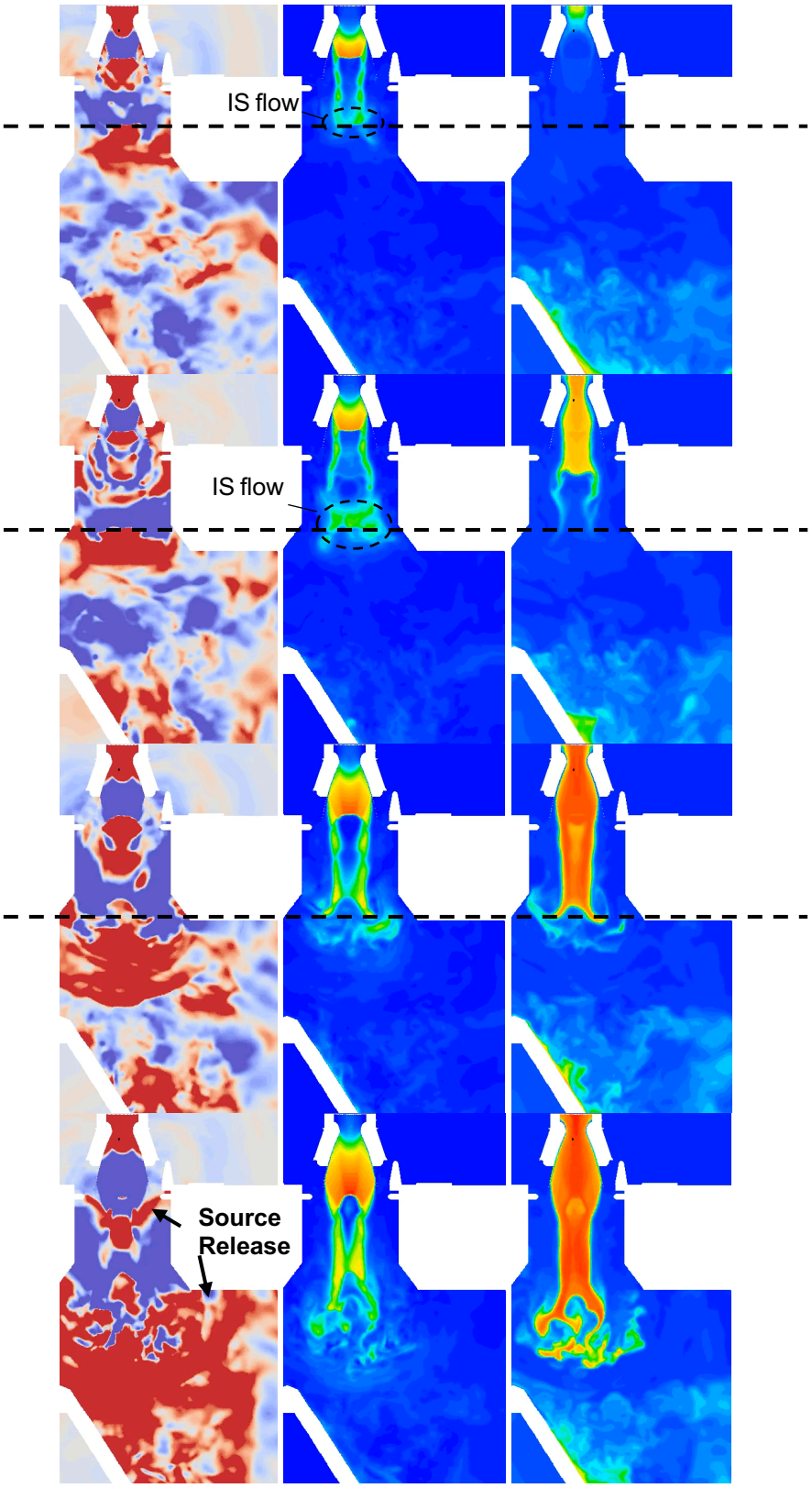

Fig. 17 Formation of the IOP1 source in a dry simulation. Gauge pressure (left), Mach number (middle), and total temperature (right).

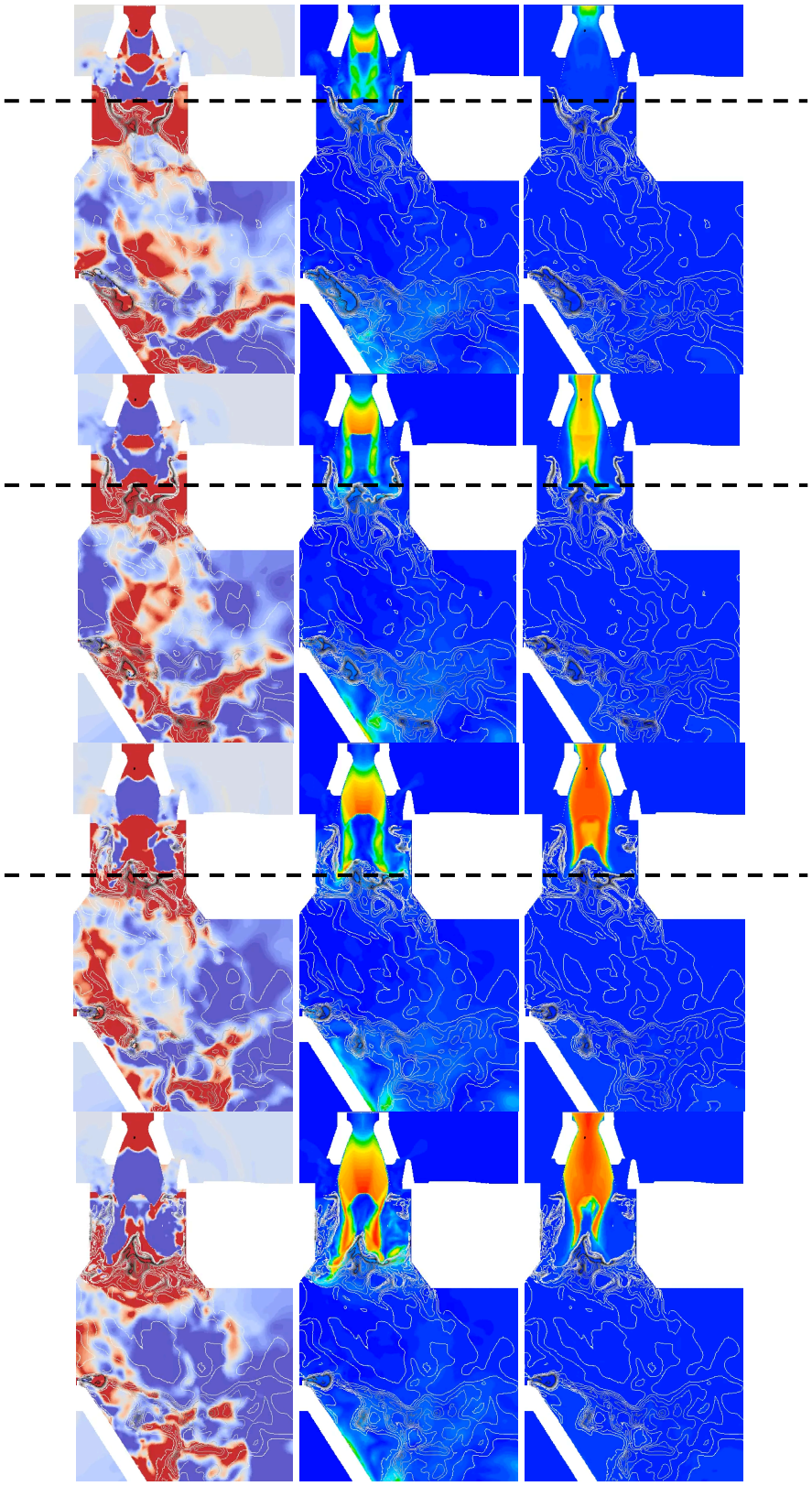

Fig. 18 Formation of the IOP1 source in the Min RF simulation (1/2). Gauge pressure (left), Mach number (middle), and total temperature (right).

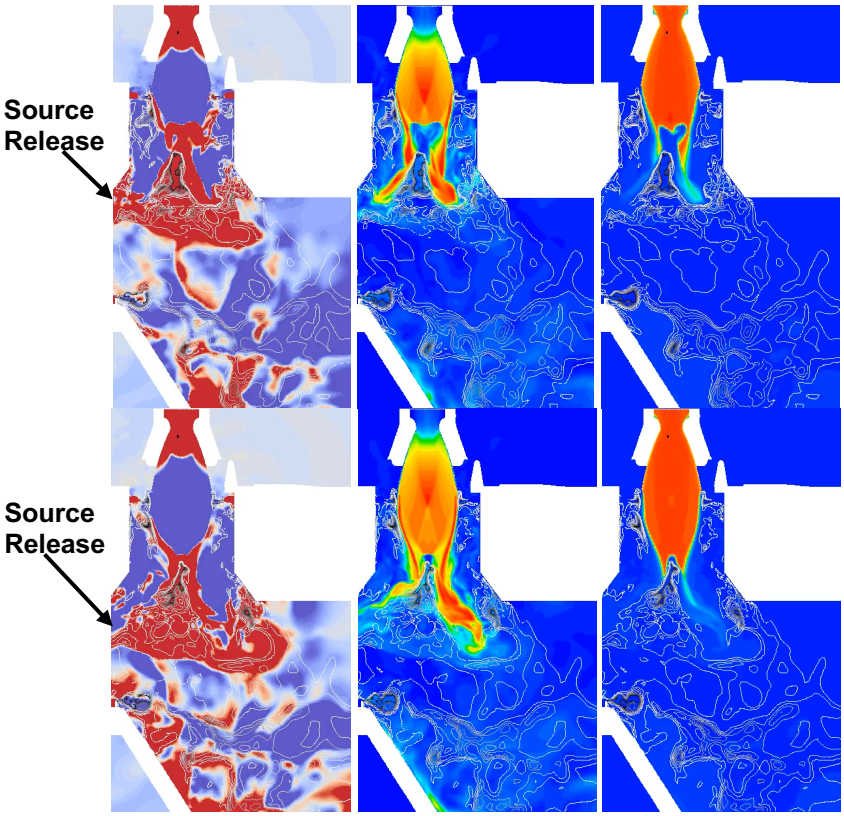

Fig. 19 Formation of the IOP1 source in the Min RF simulation (2/2). Gauge pressure (left), Mach number (middle), and total temperature (right).

A comparison between the formation and release of the pressure source forming the IOP1 wave for both dry and wet simulations is enlightening. In the dry simulation, the formation and subsequent release of the pressure source coincides with 1) the hot combustion gases overtaking the cold IS flow, 2) the intensification of the plume, and 3) the pressure source diffracting into the larger trench volume. In the wet simulation, the hot combustion gases overtake the cold IS flow and the plume intensifies seemingly without release of a pressure source. Therefore, it is possible that IOP1 is the upwards-traveling wave resulting from the diffraction of the downwards-releasing pressure source as it expands out of the MLH duct. It also appears the IOP/SS water mitigates the upward traveling IOP wave by preventing it from traveling upstream towards the vehicle. With the current level of analysis, there is not enough understanding to preclude other options, such as water absorbing energy from the plume through evaporation or displacement.

The time range showing the formation of the IOP2 source is provided in equal time increments for the dry simulation in Fig. 20 and the wet Min RF simulation in Fig. 21. It should be noted that the time increment between the wet frames is double that of the dry frames. For both figures, the left image is of gauge pressure while the right image is of Mach number.

For both simulations, the SRB plume advances through the bottom of the MLH and towards the main flame deflector (MFD). The dry simulation plume proceeds unimpeded to the MFD where it then turns horizontally into the flame trench. In the wet simulation, the SRB plume advects the IOP/SS water from the MLH downwards before encountering the water sheets being injected from the crest of the MFD. The SRB plume eventually displaces both the remaining IOP/SS water and MFD crest water to impinge on the MFD. For both simulations, shortly after the plume is turned by the MFD into the flame trench (towards the right in these images), the trench pressurizes similarly to the MLH as the SRB plumes accelerate and compress the downstream flow in the trench. Once this pressure source releases, a portion of it travels upstream into the MLH and towards the vehicle, which is the IOP2 wave identified in Fig. 16. The wet Min RF IOP2 wave is significantly delayed by the presence of the water compared to the dry IOP2 wave and approximately an order lower in magnitude.

It should be noted that unlike the IOP1 wave, the IOP2 wave does travel up the MLH duct. It is currently unclear why this is the case, though possibilities include the water altering the IOP1 source release or differences in the wave release locations. Further investigation is needed.

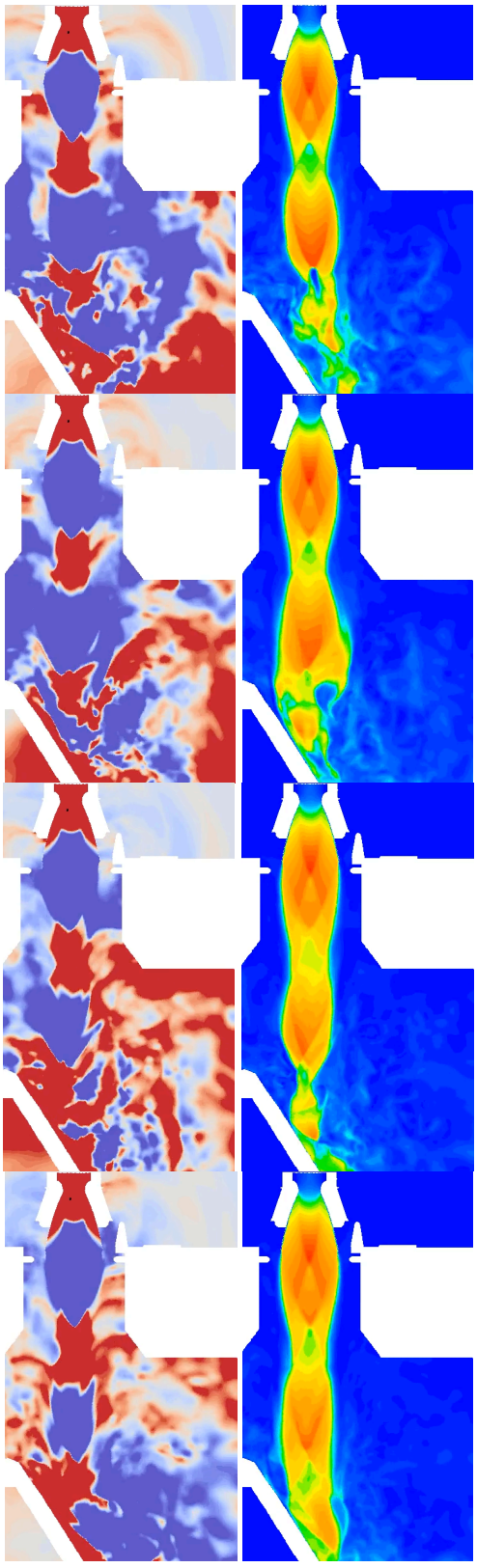

Fig. 20 Formation of the IOP2 source in a dry simulation. Gauge pressure (left) and Mach number (right).

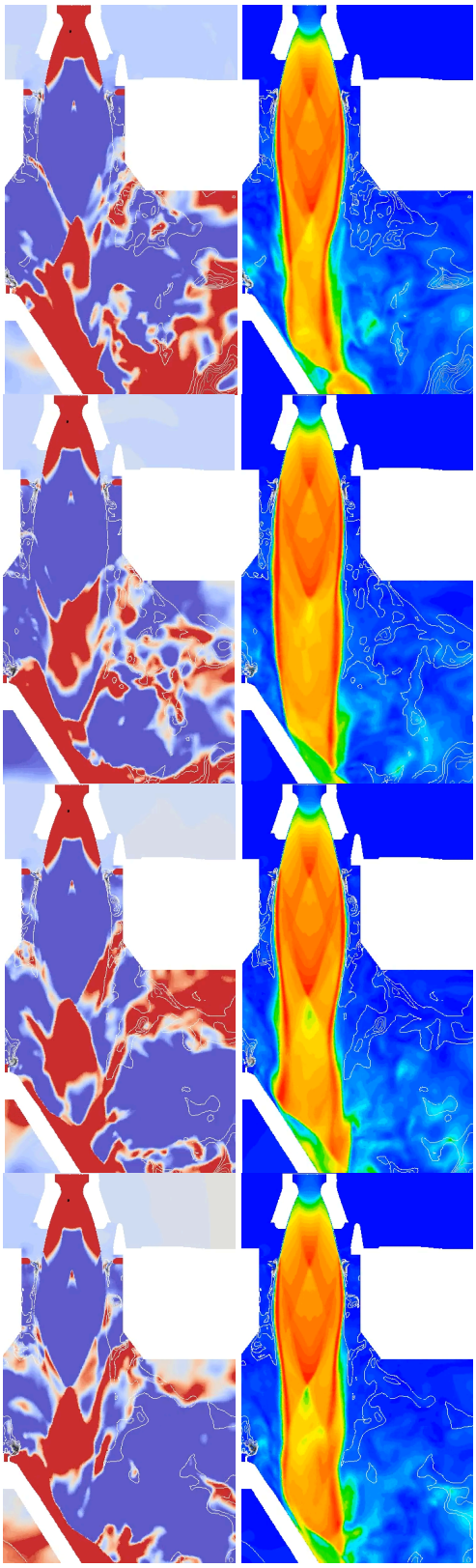

Fig. 21 Formation of the IOP2 source in the Min RF simulation. Gauge pressure (left) and Mach number (right).

Focusing again on the three wet simulations, Fig. 22 and Fig. 23 provide gauge pressure with density iso-lines for the portion of the SRB transient from igniter shock flow through the formation of the IOP1 source. The Min VoF solution is on the left, the Min RF solution is in the middle, and the Max RF solution is on the right. The same times as those provided in Fig. 18 and Fig. 19 are presented, and the Min RF solutions are duplicates provided for comparison to the other two multiphase simulations. The three multiphase simulations all show similar formation of the IOP1 source. The SRB plume moves downwards pressurizing the MLH that releases downwards with no upward-traveling portion of the wave.

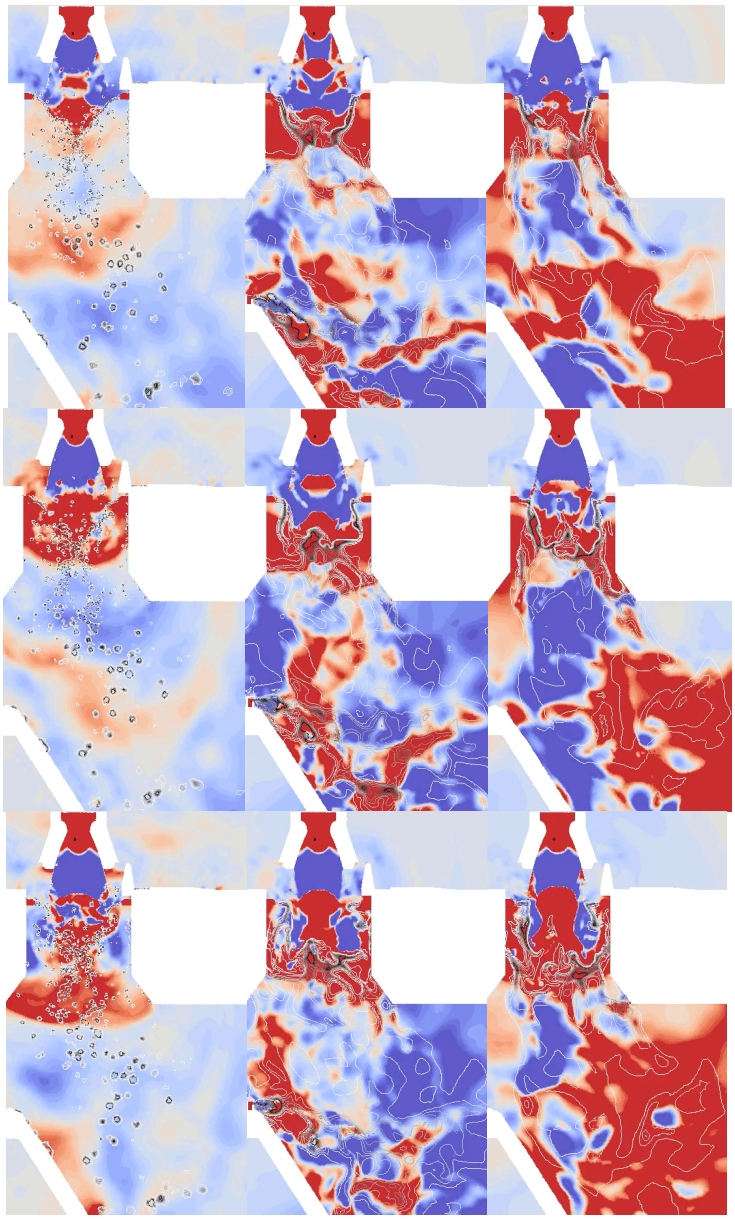

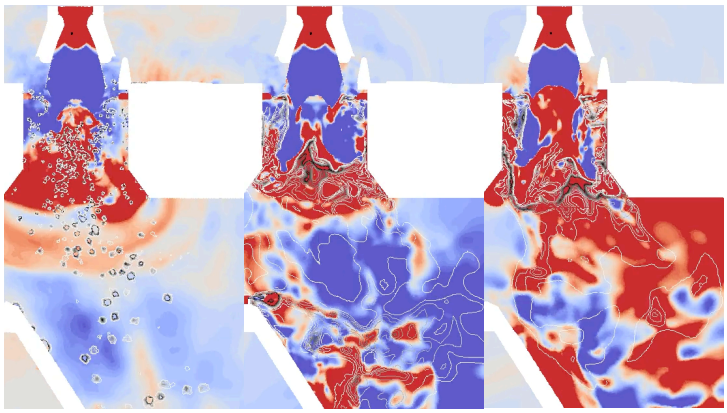

Fig. 22 Formation of the IOP1 source in gauge pressure for all three multiphase simulations (1/2). Min VoF (left), Min RF (middle), and Max RF (right).

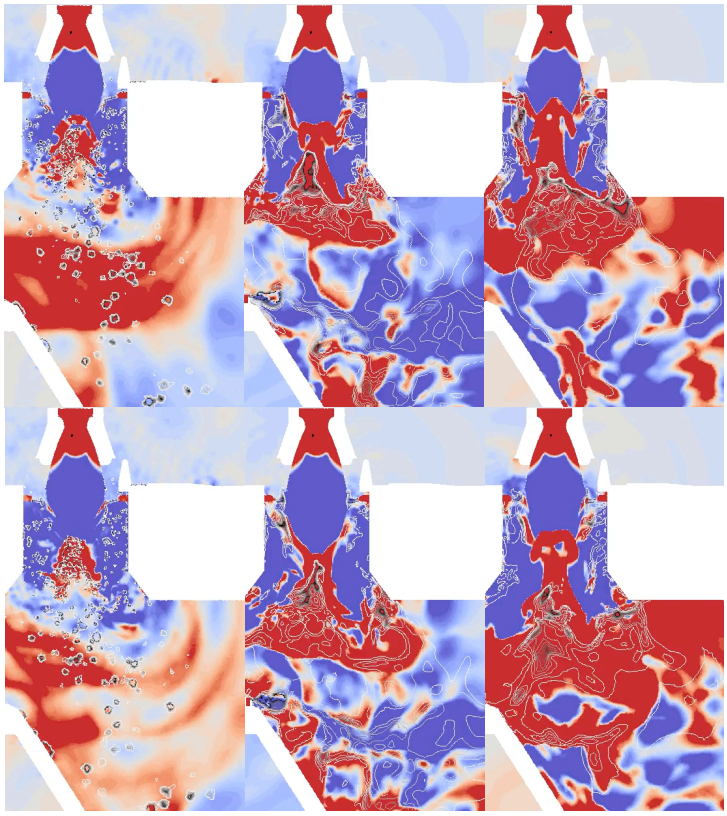

Fig. 23 Formation of the IOP1 source in gauge pressure for all three multiphase simulations (2/2). Min VoF (left), Min RF (middle), and Max RF (right).

It was elected not to compare the formation of the IOP2 wave identified in Fig. 16 to the Min VoF and Max RF simulations in this paper. Only the Min RF simulation, compared to the dry simulation above, was executed with the MFD crest water. As seen in Fig. 20 and Fig. 21, the SRB plume propagation is impeded by the crest water which would have a first order effect on the formation of the IOP2 source.

Though it is difficult to determine which wave (or waves) in the flight data is IOP, it is apparent that the SLS IOP/SS water effectively mitigated the magnitude of IOP and that the Loci/CHEM-RF and Loci/STREAM-VoF multiphase simulations mimic this effect. The pressure magnitudes predicted by the multiphase simulations are similar to those recorded in flight, as demonstrated by Fig. 14. Additionally, the Min RF simulation was demonstrated to reduce the magnitude of the IOP waves by approximately an order of magnitude, which is also reflected in the other two multiphase simulations. The agreement of the CFD with the Artemis I flight data through the early SRB transient

as well as the IOP magnitude reduction provides partial validation for the application of the Loci/CHEM-RF and Loci/STREAM-VoF multiphase CFD tools to the SLS multiphase launch environment.

IV. Conclusion

The SLS program uses an IOP/SS water system to reduce the SRB-generated IOP and other liftoff acoustics loads. Subscale testing and heritage data from the Shuttle program gave confidence in the expected acoustic mitigation effects from the SLS IOP/SS water design, but there was some uncertainty regarding other portions of the SLS launch environment due to configuration differences between Shuttle, the subscale test, and SLS. Because no full integrated system SLS testing was conducted prior to launch, computational fluid dynamics (CFD) was relied upon to inform the SLS program on the multiphase launch environment in areas including but not limited to RS-25 lead hydrogen burn-off igniters (HBOIs) operation, water system design, debris transport, and environment development.

With the November 2022 launch of the SLS vehicle during the Artemis I mission, these predictive CFD simulations could be compared to flight data to assess their validity. Of the five multiphase simulations available, three were compared to the flight data as they most closely matched the day of launch conditions. One of the simulations was executed with the Loci/STREAM-Volume of Fluid (VoF) solver while the other two were executed with the Loci/CHEM-Real Fluids (RF) CFD solver.

Qualitative validation was achieved by comparing the CFD flowfields to Artemis I flight video. Both solvers were found to successfully predict the plume-water interaction where the SRB plume initially stagnates on the IOP/SS water sheets and turns outwards in all directions, including towards the RS-25 engines. Outward velocity jets in the CFD simulations were found to compare well to video evidence of outwards water spray.

Quantitative validation of the environment prediction was achieved by comparing Artemis I pressure data at the SLS Core Stage base heat shield to CFD pressure data at the same location. All three CFD simulations successfully predicted the SRB igniter shock, secondary igniter shock, and the magnitude of the IOP mitigation effect from the water. Examination of the CFD flowfields indicated that the IOP source forms as the MLH pressurization diffracts from the confined MLH duct into the larger flame trench volume. Additionally, a secondary IOP wave was found to form as the flame trench is pressurized by the SRB plume. Though more work is needed to understand the formation and propagation of these IOP waves in the multiphase environment, the CFD simulations suggest that the water mitigates IOP by preventing or impeding the upward traveling portion of the pressure sources that form in the MLH and flame trench.

The results of this analysis substantiate the successful validation of both the Loci/STREAM-VoF and Loci/CHEM-RF CFD solvers for prediction of the IS wave and IOP magnitude in a complex multiphase environment, and provide confidence in the application of these tools to future variants of the SLS vehicle as well as other heavy lift launch vehicles.

References

[1] Jones, J., Guest, S, Nesman, T., Matienzo, J., and Reed, D., "Acoustic, Overpressure and Unsteady Flow Phenomena Associated with the Saturn/Space Shuttle Systems: A Review of Selected Issues," In *Symposium on "Acoustical and Dynamic Environment of Space Transportation Systems,"* February 1994.

[2] Rivord, T. and Williams, B., "Validation of SLS Launchpad Water and Plume-water Induced Side Loads," *JANNAF*, June 2022.

[3] L. Strutzenberg. ER42 (14-133), "SLS DAC3 Geometry for CFD: RS-25 and Booster Nozzle Internal." Huntsville, AL, December 2014.

[4] L. Strutzenberg. ER42 (14-037), "Delivered SLS DAC3 Integrated Pad ML 10005 Geometry for CFD Part 1: Deck Plume Impingement." Huntsville, AL, December 2014.

[5] T. Drake., "Transmittal Memorandum-SBU and RFTU, IOP/SS Water Flow Rate Schedule Interdependency 1032: Water Nozzle CAD geometry; Interdependency 1033.", 15 March 2017.